Photon-assisted thermoelectric properties of noncollinear spin valves

Xiaobin Chen, Dongping Liu, Wenhui Duan, and Hong Guo

Phys. Rev. B **87**, 085427 — Published 19 February 2013

DOI: 10.1103/PhysRevB.87.085427

Photon-assisted thermoelectric properties of noncollinear spin-valves

Xiaobin Chen[1,2,*] Dongping Liu[2], Wenhui Duan[1], and Hong Guo[2]
[1]*Department of Physics and State Key Laboratory of Low-Dimensional Quantum Physics, Tsinghua University, Beijing 100084, People's Republic of China*
[2] *Department of Physics, Center for the Physics of Materials, McGill University, Montréal, Québec H3A 2T8, Canada*
(Dated: February 4, 2013)

We report theoretical analysis of thermal-spin and thermoelectric properties of noncollinear spin-valves driven by a high frequency AC voltage bias. The spin-valve consists of two ferromagnetic contacts sandwiching a single-level or multi-level quantum dot (QD). A general formulation for the time-averaged thermal-spin and thermoelectric properties of spin-valves is derived within the nonequilibrium Green's function theory, which provides a starting point for further numerical calculations of these properties. Numerical results of a spin-valve having a spin-degenerate single-level QD are given as an example. The AC bias induces various photon-assisted transmission peaks which can greatly enhance the Seebeck coefficients and the figures of merit, and offer a new possibility to tune both the spin-dependent and normal thermoelectric properties of the spin-valve. Details of these properties and how they depend on the non-collinearity of the spin-valve, magnetic polarization, temperature, AC bias, and other control parameters are reported. A particularly interesting result is the opposite dependency of the thermoelectric properties on the magnetic polarization and non-collinearity for contacts with or without spin accumulation.

I. INTRODUCTION

Concerns about the deteriorating global environment and depleting natural resources have prompted a new wave of technology development for green energy solutions in which the century-old phenomenon of thermoelectric effects has regained particular prominence.[1–5] Thermoelectricity converts heat to electricity or vice versa, thus has been used in harvesting waste heat in industrial processes and in on-chip cooling for integrated circuits.[6–8] The maximum conversion efficiency of thermoelectricity is measured by a dimensionless figure of merit called ZT coefficient, defined as $ZT \equiv GS^2T/(k_e + k_{ph})$, where G is the electric conductance, S is the Seebeck coefficient, k_e the electronic thermal conductance, and k_{ph} the lattice thermal conductance of the thermoelectric material. The relentless search for methods and materials to increase ZT has been going on for over a century. The highest value of ZT for *bulk* materials is about unity which appears to be difficult to increase further because of the Wiedemann-Franz Law[9] that dictates $G \propto k_e$, thus any increase of electric conductance G is not automatically translated into an increase of ZT due to the balancing effect of thermal conductance k - especially in metals; and due to the relatively large lattice thermal conductance accompanied with limited value of S^2G in semiconductors. Recognizing this problem, recent efforts have been shifted toward nano-structured materials (as opposed to bulk materials) where lattice thermal conductance can be diminished and much larger ZT may be possible.[1,10]

Besides exploiting the nano-structured materials to decrease the lattice thermal conductance, their electronic properties can also be manipulated to increase ZT. According to Mott's relation,[11–13] in the linear response regime the Seebeck coefficient $S \approx \left(-\pi^2 k_B^2 T/3|e|\right) [\ln \mathcal{T}(\varepsilon)]'_\varepsilon|_{\varepsilon=\mu}$, where $[\ln \mathcal{T}(\varepsilon)]'_\varepsilon|_{\varepsilon=\mu}$ is the energy derivative of $\ln \mathcal{T}(\varepsilon)$ at the electrochemical potential μ, $\mathcal{T}(\varepsilon)$ is the transmission function. Therefore, a sharp conductance peak versus energy around the electrochemical potential should greatly enhance S, thereby improving the figure of merit ZT.[14,15] In this regard and according to Mahan and Sofo, the best ZT for a given lattice thermal conductivity can be achieved by a δ-function like transmission coefficient.[16] For bulk materials, it is difficult to realize δ-function like transmission; but for nanostructures such as quantum dots (QDs) having discrete energy levels, the transmission coefficient $\mathcal{T}(\varepsilon)$ versus energy ε exhibits a Lorentzian line shape around each level, which can be viewed as broadened δ-like line shapes. The peak positions of $\mathcal{T}(\varepsilon)$ in QD devices can also be tuned conveniently by a gate voltage to align with the electrochemical potential μ so that an enhanced Seebeck coefficient is achieved. Nanostructures such as QD systems also provide new opportunities toward manipulating currents and/or achieving spin-accumulation by the thermoelectrical effects.

More recently, two very interesting research directions of thermoelectricity of nanostructures have been pursued. The first is the spin caloritronics[4,17] which studies thermoelectricity in spintronic devices and magnetic structures. The second is the photon-assisted heat transport which studies thermoelectricity under time-dependent electromagnetic radiation at very low temperatures when phonons are largely frozen.[18–21] Most recently, Zhang *et al.*[22] reported an experimental discovery of a novel Seebeck rectification and frequency-dependent transport measurements at GHz frequency for magnetic tunnel junctions (MTJ). Zhang *et al.*'s work is the first to explore the possibility of utilizing spin caloritronics in high-frequency applications. Motivated by this very interesting experiment and the research direction it represents, in this work we theoretically analyze both the conventional and the spin-dependent Seebeck coefficients in spin-valves with non-collinear magnetic structure, under high frequency AC voltage bias.

A MTJ is a spin-valve structure where two ferromagnetic (FM) contacts sandwich a non-magnetic space layer,[23] as schematically shown in Fig. 1. In our work, the non-magnetic spacer is replaced by a QD. By varying the relative angle θ which measures the non-collinearity between the magnetic moments of the two contacts, the electric current and spin current can be continuously modulated between a maximum at $\theta = 0$ and a minimum at $\theta = \pi$.[24,25] Replacing the space layer by a QD is interesting because of resonant tunneling which typically gives rise to sharp peaks in the transmission coefficients. Furthermore, clearly resolved photon-assisted side peaks in resonant tunneling in QDs under GHz[28–30] and THz radiations[31] have been observed experimentally. Therefore, it is possible to tune the peak positions by photon-assisted processes driven by AC fields to enhance the Seebeck coefficient.

Theoretical investigations of thermoelectric effects in MTJ or under AC fields have discovered rich properties in QD models having non-collinear ferromagnetic contacts in DC fields,[26,27] or models having non-magnetic contacts in AC fields.[21] Our work focuses on the most general situation of QD based non-collinear spin-valves in AC fields. In particular, we note that frequency dependent features of thermoelectric properties of the non-collinear spin-valves have not been theoretically investigated and this work reports the necessary theoretical formalism and numerical analysis for understanding these properties.

We begin by deriving general expressions for the spin-resolved electric current and thermoelectric properties of FM/QD/FM spin-valve structure under both the DC and AC driving fields, based on the Keldysh nonequilibrium Green's function (NEGF) formalism. Analytical expressions for the charge (S_c) and spin-dependent Seebeck coefficients (S_s), the charge (Z_cT) and spin figure of merit (Z_sT), as well as normal Seebeck coefficient (S) and figure of merit (ZT), are derived in terms of spin-resolved transmission coefficients $\mathcal{T}_\sigma(\varepsilon)$, which is expressed in terms of the Green's functions of the spin-valve that can be calculated from the Hamiltonian of the device. Based on the analytical formulation, we have calculated the influence of the AC bias on transmission, Seebeck coefficients, and figures of merit as functions of the non-collinearity θ, the electron energy, and the AC frequency ω, for the FM/QD/FM spin-valve.

Our results clearly show that the AC field induces side peaks evenly distributed at energies $\hbar\omega$ in the time-averaged $\mathcal{T}(\varepsilon)$, which induces significant variation to both thermal-spin properties and thermal-charge properties of the spin-valve. We report

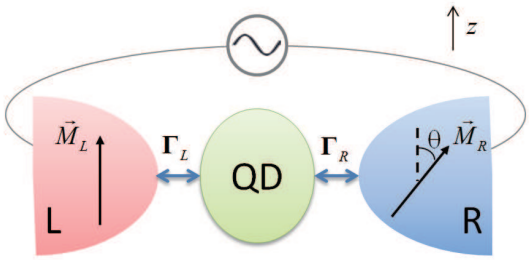

FIG. 1. (color online) Schematic plot of a two probe spin-valve device consisting of a QD connected to FM leads with noncollinear magnetic moments. An AC bias is applied across the leads.

a very interesting opposite dependency of the thermoelectric property against magnetic non-collinearity for situations with or without spin accumulation in the FM contacts. For the case with spin accumulation, there is an induced spin voltage that acts as a third driving force - in addition to the external bias voltage and the temperature gradient, to determine the charge Seebeck coefficient S_c via an average of the individual Seebeck coefficients of the two spin channels. It is shown that S_c generally achieves its maximum when $\theta = 0$ (parallel spin-valve configuration, PC). For the case without spin accumulation in the FM contacts, the relevant quantity is the normal Seebeck coefficient which we find to usually has its maximum at $\theta = \pi$ (anti-parallel configuration, APC), consistent with several available experiments[5,22,32] - implying no spin accumulation effect in those experiments. The Seebeck coefficients (including the spin-dependent Seebeck coefficient) are found to have negligible change when AC frequency ω is small, but at larger ω in and beyond the microwave range, the Seebeck coefficients oscillate around its DC value before going back to the DC value after $\omega > |\varepsilon_0 - \mu|$. Using reasonable materials and device parameters which correspond to those in typical QD experiments, the calculated Seebeck coefficients are consistent to the experimentally reported values.[22] Most importantly, the predicted oscillation in Seebeck coefficients of the spin-valves also results in an similar oscillation in ZT, suggesting a fascinating possibility to tune relevant thermoelectric properties of spintronic systems by noncollinearity and AC fields.

The rest of the paper is organized as follows. In Section II, general formulae for the charge and spin transport properties of a multi-level noncollinear spin-valve under AC bias are derived using the NEGF technique. Specifically, we focus on the time-averaged expressions for the thermal-spin and thermoelectric properties. These analytical expressions are applied in Section III to a spin degenerate single-level spin-valve system, where the general, qualitative behaviors are investigated first. Afterward, the angular, polarization, and frequency dependencies of the thermal-spin and thermoelectric properties are carefully investigated using realistic materials and device parameters. Finally, a conclusion is drawn in Section IV. To simplify the presentation, we organize the details of the theoretical analysis into several Appendices.

II. THEORETICAL ANALYSIS

In this section, we present analytical derivations based on NEGF formalism of various Seebeck coefficients and the figures of merit for the noncollinear FM/QD/FM spin-valve under an external AC bias voltage.

A. The Hamiltonian of the device model

We consider a typical FM/QD/FM spin-valve as shown in Fig. 1. For a multi-level QD connected to FM leads with non-collinear magnetic moments under AC bias, the Hamiltonian can be written in the following form,[33]

$$H = H_L + H_R + H_C + H_T, \tag{1}$$

$$H_L = \sum_{\sigma,k,\alpha\in L} \left[E_{k\alpha}(t) + \sigma M_L\right] c^\dagger_{k\alpha\sigma} c_{k\alpha\sigma}, \tag{2}$$

$$H_C = \sum_{n\sigma} \varepsilon_{n\sigma} d^\dagger_{n\sigma} d_{n\sigma}, \tag{3}$$

$$\begin{aligned} H_R = & \sum_{\sigma,k,\alpha\in R} \left[E_{k\alpha}(t) + \sigma M_R \cos\theta\right] c^\dagger_{k\alpha\sigma} c_{k\alpha\sigma} \\ & + \sum_{\sigma,k,\alpha\in R} M_R \sin\theta c^\dagger_{k\alpha\sigma} c_{k\alpha\bar{\sigma}}, \end{aligned} \tag{4}$$

$$H_T = \sum_{\sigma,n,k,\alpha\in L,R} \left(T_{k\alpha,n} c^\dagger_{k\alpha\sigma} d_{n\sigma} + H.c.\right), \tag{5}$$

where $c^\dagger_{k\alpha\sigma}$ ($c_{k\alpha\sigma}$) creates (annihilates) an electron with spin-σ and Bloch wavevector k in energy band α of the leads, while $d^\dagger_{n\sigma}$ ($d_{n\sigma}$) creates (annihilates) an electron of spin σ occupying level n in the QD. $\sigma = \uparrow, \downarrow$ labels the spin eigenstates along z axis; $\bar{\sigma} = -\sigma$, i.e., $\bar{\sigma} \uparrow$ if $\sigma = \downarrow$, and vice versa. $E_{k\alpha}(t) = E^0_{k\alpha} + \Delta_\alpha(t) = E^0_{k\alpha} - e\Delta_\alpha \cos\omega t$ ($-e$ the electron charge) when a harmonic AC bias is applied. This AC model which includes the influence of AC fields by modifying the energy levels of the isolated leads, was originally proposed by Jauho *et al.*,[34] and has been successfully used by Sun *et al.*[35] to explain the experimentally observed resonant structures of average current vs gate voltage when a microwave field is shed on one lead of a tunneling QD.[28] H_T is the hopping term between the QD and the leads. As shown in Fig. 1, the magnetic moment $\vec{M}_L$ of the left lead (L) is aligned with the z axis, while that of the right lead (R), $\vec{M}_R$, has a tilted angle θ with the z axis, forming a noncollinear magnetic configuration. Misalignment between $\vec{M}_L$ and $\vec{M}_R$, i.e., for $\theta \neq 0, \pi$, introduces an effective spin-flip process as shown in H_R. Transforming the reference axis into the spin quantization axis along $\vec{M}_R$, lead R turns from an interacting lead to a non-interacting lead as

$$H_R = \sum_{\substack{k,\alpha\in R \\ s=+,-}} \left[E_{k\alpha}(t) + sM_\alpha\right] C^\dagger_{k\alpha s} C_{k\alpha s}, \tag{6}$$

where the spin indices $s = +, -$ denote the spin eigenstates along the direction of $\vec{M}_R$, and $C^\dagger_{k\alpha s}$ ($C_{k\alpha s}$) creates (annihilates) an electron labeled by ($k\alpha s$) in lead R. The hopping term is now

$$\begin{aligned} H_T = & \sum_{n,k\alpha\in R} (T_{k\alpha,n} \cos\frac{\theta}{2} C^\dagger_{k\alpha+} d_{n\uparrow} - T_{k\alpha,n} \sin\frac{\theta}{2} C^\dagger_{k\alpha-} d_{n\uparrow} \\ & + T_{k\alpha,n} \cos\frac{\theta}{2} C^\dagger_{k\alpha-} d_{n\downarrow} + T_{k\alpha,n} \sin\frac{\theta}{2} C^\dagger_{k\alpha+} d_{n\downarrow} + H.c.) \\ & + \sum_{n,\sigma,k\alpha\in L} \left(T_{k\alpha,n} c^\dagger_{k\alpha\sigma} d_{n\sigma} + H.c.\right) \\ \equiv & \sum_{k\alpha s,n\sigma} \left(t_{k\alpha s,n\sigma} C^\dagger_{k\alpha s} d_{n\sigma} + H.c.\right), \end{aligned} \tag{7}$$

where for compactness, we let $C^{(\dagger)}_{k\alpha+(-)} = c^{(\dagger)}_{k\alpha\uparrow(\downarrow)}$ in lead L. Note that in the above and as is typical, the tunneling coupling parameter $T_{k\alpha,n}$ is assumed to be spin-independent.[33,36] With these manipulations, the two-probe FM/QD/FM device model under the AC driving field is specified by the Hamiltonian of Eqs. (1)-(3), (6), and (7).

In the NEGF derivations of transport properties such as the spin polarized current, the FM/QD/FM two-probe structure is divided into three regions: the left/right FM leads and the QD. By integrating out the degrees of freedom (i.e., the operators) of the leads, one focuses on the NEGF of the QD. In this way, the effects due to the leads on the QD are included into a set of self-energies. Following Ref. 33, the self-energies due to the noncollinear FM leads are found to be

$$\Sigma^\gamma_R = V^\dagger g^\gamma_R V = \mathbf{R}^\dagger \Sigma^\gamma_{R0} \mathbf{R}, \quad \Sigma^\gamma_L = \Sigma^\gamma_{L0}, \tag{8}$$

where $\gamma = r, a, <$ indicates retarded, advanced, and lesser quantities; subscripts R, L indicate the left, right leads; g^γ is the surface Green's function of the semi-infinite leads; and $\mathbf{R}$ is the rotation matrix:

$$\mathbf{R} = \begin{pmatrix} \cos\theta/2 & \sin\theta/2 \\ -\sin\theta/2 & \cos\theta/2 \end{pmatrix}. \tag{9}$$

The quantities $\Sigma^{\gamma}_{\alpha 0}$ ($\alpha = L, R$) above are defined as

$$\Sigma^{\gamma}_{\alpha 0} \equiv \begin{pmatrix} \Sigma^{\gamma}_{\alpha 0\uparrow} & 0 \\ 0 & \Sigma^{\gamma}_{\alpha 0\downarrow} \end{pmatrix}, \quad \Sigma^{\gamma}_{\alpha 0\sigma;m,n} = \sum_{k,\beta\in\alpha} T_{k\beta,n} T^{*}_{k\beta,m} g^{\gamma}_{R;k\beta\sigma}, \tag{10}$$

which is the self-energy of lead α when $\vec{M}_{\alpha}$ is parallel with z axis. The time variables due to the external AC fields applied on the leads (see Eqs. (2) and (6)) are not written out explicitly in the self-energies.

The self-energies can be transformed into energy space to facilitate further derivations and, for simplification of analysis, the wide-band limit (WBL) will be applied. This is an approximation that amounts to neglecting the energy dependence of the coupling between the leads and the QD, which is reasonable since the leads are made of good metals. In WBL, the retarded self-energy can be expressed in terms of bandwidth functions as[33,34]

$$\Sigma^{r}_{\alpha}(\varepsilon) \approx -\frac{i}{2}\mathbf{\Gamma}_{\alpha},$$

where

$$\mathbf{\Gamma}_{R} = \mathbf{R}^{\dagger}\begin{pmatrix} \Gamma_{R\uparrow} & 0 \\ 0 & \Gamma_{R\downarrow} \end{pmatrix}\mathbf{R}, \quad \mathbf{\Gamma}_{L} = \begin{pmatrix} \Gamma_{L\uparrow} & 0 \\ 0 & \Gamma_{L\downarrow} \end{pmatrix} \tag{11}$$

with boldface notation $\mathbf{\Gamma}$ to denote a full matrix of the bandwidth function. The original matrix elements of $\Gamma_{\alpha\sigma}$ are

$$[\Gamma_{\alpha\sigma}(\varepsilon)]_{m,n} \equiv 2\pi \sum_{\beta\in\alpha} \rho_{\beta\sigma}(\varepsilon)\, T_{\beta,n}(\varepsilon)\, T^{*}_{\beta,m}(\varepsilon)\ .$$

Here $T_{\beta,n}(\varepsilon_k) = T_{k\beta,n}$, $\alpha = L/R$ is the label for either of the two FM leads, and $\rho_{\beta\sigma}(\varepsilon)$ is the spin density of states (DOS) as a function of energy in lead α for spin-channel σ.

If there is one energy level in the QD and consider a channel in the leads, from its definition and the fact that $T_{k\alpha,n}$ is free of spin labels, we observe that

$$\Gamma_{\alpha\uparrow}(\varepsilon)/\Gamma_{\alpha\downarrow}(\varepsilon) = \rho_{\alpha\uparrow}(\varepsilon)/\rho_{\alpha\downarrow}(\varepsilon).$$

Consequently, by introducing the spin polarization as

$$p_{\alpha} \equiv \frac{\rho_{\alpha\uparrow}(\varepsilon) - \rho_{\alpha\downarrow}(\varepsilon)}{\rho_{\alpha\uparrow}(\varepsilon) + \rho_{\alpha\downarrow}(\varepsilon)},$$

we obtain[37,38]

$$\Gamma_{\alpha,\sigma}(\varepsilon) = \Gamma_{\alpha}(1 + \sigma p_{\alpha}) \tag{12}$$

with

$$\Gamma_{\alpha} = 2\pi |T_{\alpha,d}(\varepsilon)|^{2}\left[\rho_{\alpha\uparrow}(\varepsilon) + \rho_{\alpha\downarrow}(\varepsilon)\right],$$

and $\sigma = \uparrow, \downarrow$ denoting different spin channels. Herein, spin-up ($\sigma = \uparrow$) is assumed to be the majority spin channel.

For time-dependent cases, the self-energies still can be related to the time-independent bandwidth matrices (Eq. (11)) as indicated by Eqs. (B2) and (C1) in the appendices.

B. Spin polarized current

From the device model specified by the Hamiltonian Eqs. (1)-(3), (6), and (7), the electric current contributed by spin-s ($s = +, -$, denoting the spin eigenstates of local spin quantization axis) electrons in lead L under the WBL is given by the following expression (for detailed derivations, see Appendix A, $\hbar = 1$):

$$\begin{aligned} J_{L,s} = -2e\,\mathrm{Tr}\,\mathrm{Im}\Bigg\{ \int \frac{d\varepsilon}{2\pi}\mathbf{\Gamma}_{Ls} \int_{-\infty}^{t} d\tau_1 G^{r}(t,\tau_1)\cdot f_{L}(\varepsilon) \\ \times\ e^{-i\varepsilon(\tau_1 - t)} e^{-i\int_{t}^{\tau_1}\Delta_{L}(\tau)d\tau}\Bigg\} - e\,\mathrm{Tr}\,\mathrm{Im}\,\mathbf{\Gamma}_{Ls} G^{<}(t,t), \end{aligned} \tag{13}$$

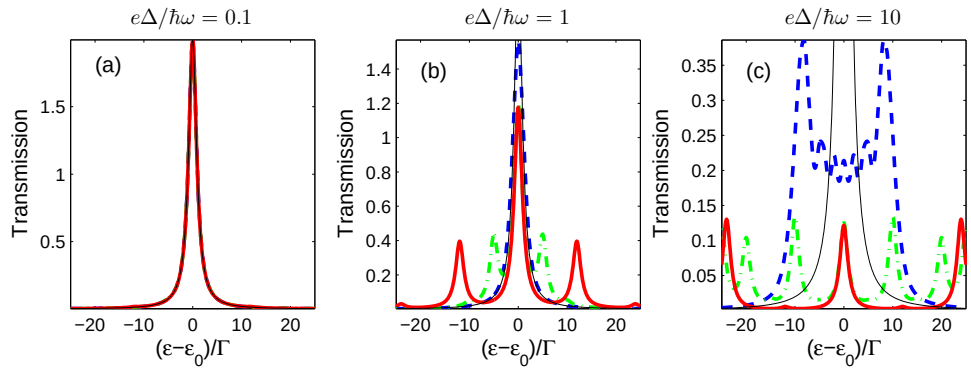

FIG. 2. (color online) Total transmission coefficients, $\mathcal{T}(\varepsilon)$, of a non-polarized ($p = 0$) single-level FM/QD/FM device in parallel configuration ($\theta = 0$) and under AC bias with $\hbar\omega/\Gamma = 1$ (blue dashed line), 5 (green dash dotted line), 12 (red solid thick line), and without AC bias (black solid thin line) for $e\Delta/\hbar\omega$ = (a) 0.1, (b) 1, and (c) 10, respectively.

where $\mathbf{\Gamma}_{Ls}$ is the spin-s bandwidth matrix of lead L, and its elements are defined as

$$(\mathbf{\Gamma}_{Ls})_{n'\sigma',n\sigma} \equiv 2\pi \sum_{\alpha\in L} \rho_{\alpha s}(\varepsilon)\, t_{\alpha s,n\sigma}(\varepsilon)\, t^{*}_{\alpha s,n'\sigma'}(\varepsilon).$$

Eq. (13) is a simple extension of the charge current derived in Ref. 34. If both $\vec{M}_L$ and $\vec{M}_R$ are aligned collinearly to the z axis (PC or APC), all quantities become diagonalized in spin space. Furthermore, if there is no AC current, Eq. (13) reduces to those derived in Refs. 39 and 40, namely

$$J_{L,s} = e\left\{\int \frac{d\varepsilon}{2\pi}\left[f_L(\varepsilon) - f_R(\varepsilon)\right] \mathrm{Tr}[\Gamma_{L,s} G^r_s(\varepsilon)\, \Gamma_{R,s} G^a_s(\varepsilon)]\right\},$$

where the trace goes over the orbital degrees of freedom.

As mentioned before, we assume the magnetic moment of the left lead $\vec{M}_L$ to be parallel with the z axis. Therefore, the spin-s bandwidth matrices of lead L are diagonalized in spin space,

$$\mathbf{\Gamma}_{L+} = \begin{pmatrix} \Gamma_{L\uparrow} & 0 \\ 0 & 0 \end{pmatrix}, \quad \mathbf{\Gamma}_{L-} = \begin{pmatrix} 0 & 0 \\ 0 & \Gamma_{L\downarrow} \end{pmatrix},$$

or $(\mathbf{\Gamma}_{Ls})_{\sigma'\sigma} = (\mathbf{\Gamma}_{Ls})_{\sigma'\sigma}\delta_{\sigma'\sigma}$, and $+(-) = \uparrow(\downarrow)$. In this case, the current expression (13) can be rewritten as

$$J_{L,\sigma} = -2e\,\mathrm{Im}\,\mathrm{Tr}\left\{\int \frac{d\varepsilon}{2\pi}\Gamma_{L\sigma}\int_{-\infty}^{t} d\tau_1 G^r_{\sigma\sigma}(t,\tau_1)\cdot f_L(\varepsilon) \right.$$
$$\left. \times\, e^{-i\varepsilon(\tau_1 - t)} e^{-i\int_t^{\tau_1}\Delta_L(\tau)d\tau}\right\} - e\,\mathrm{Im}\,\mathrm{Tr}\,\Gamma_{L\sigma} G^{<}_{\sigma\sigma}(t,t)\,. \tag{14}$$

Note that the trace in Eq. (13) goes over both spin and orbital degrees of freedom, while in Eq. (14), only orbital degrees of freedom.

To move forward, the retarded and lesser Green's functions must be calculated. The retarded Green's function G^r of the QD of the two-probe device is obtained from the corresponding Green's function of the isolated QD (without the leads) using the Dyson equation (for details see Appendix B),

$$G^r(t,t') = \int_{-\infty}^{+\infty} \frac{d\varepsilon}{2\pi} G^r(\varepsilon)\, e^{-i\varepsilon(t-t')}\,, \tag{15}$$

$$G^r(\varepsilon) = (\varepsilon + i\eta - H_0 + \Sigma^r)^{-1}\,. \tag{16}$$

As for the lesser Green's function $G^<$, we make utility of the Keldysh relation, $G^< = G^r\Sigma^< G^a$, which can be easily calculated once G^r is known.

In this work we are interested in the time averaged current. To this end we assume that the amplitudes of the AC bias applied to the two leads to be the same, $\Delta_L = \Delta_R \equiv \Delta$. As detailed in Appendix C, Eq. (14) is reduced to the following form:

$$J_{L,\sigma} = e\int \frac{d\varepsilon}{2\pi}\left[f_L(\varepsilon) - f_R(\varepsilon)\right] \sum_{k=-\infty}^{+\infty} J_k^2\left(\frac{e\Delta}{\omega}\right) \times$$
$$\times\, \mathrm{Tr}\left[\mathbf{\Gamma}_{L,\sigma} G^r(\varepsilon - k\omega)\, \mathbf{\Gamma}_R G^a(\varepsilon - k\omega)\right], \tag{17}$$

where J_k is the k-th order Bessel function of the first kind. When $\Delta = 0$, i.e., no AC bias is applied, Eq. (17) reduces to the familiar DC expression, $J_{L,\sigma} = e\int \frac{d\varepsilon}{2\pi}(f_L - f_R)\,\mathrm{Tr}[\mathbf{\Gamma}_{L,\sigma}G^r(\varepsilon)\mathbf{\Gamma}_R G^a(\varepsilon)]_{\sigma\sigma}$.

From Eq. (17), various physical quantities of interest are obtained. The time-averaged effective transmission coefficient of spin-σ channel is given by the main integrand of Eq. (17),

$$\mathcal{T}_\sigma(\varepsilon) = \sum_{k=-\infty}^{+\infty} J_k^2\left(\frac{e\Delta}{\omega}\right)\mathrm{Tr}\left[\mathbf{\Gamma}_{L,\sigma}G^r(\varepsilon - k\omega)\mathbf{\Gamma}_R G^a(\varepsilon - k\omega)\right]\ . \tag{18}$$

In this work, $\mathcal{T}_\sigma(\varepsilon)$ and $\mathcal{T}(\varepsilon)$ denote the transmission coefficient of spin-σ electrons and total transmission, respectively. To avoid possible confusion, the energy dependence of transmission coefficients is always written out explicitly. The spin current and charge current are obtained as the difference or sum of contributions from the two spin channels,

$$J_\mathrm{s} = J_{L,\uparrow}(t) - J_{L,\downarrow}(t)\ , \tag{19}$$

$$J_\mathrm{c} = J_{L,\uparrow}(t) + J_{L,\downarrow}(t)\ . \tag{20}$$

For the thermoelectric properties of the FM/QD/FM device, we shall distinguish two situations: with or without spin accumulation at the FM contacts.

a. With spin accumulation. Spin accumulation will generate a spin chemical potential which drives a spin current. For finite systems applied a small temperature difference, achieving equilibrium means that there should be no net spin current nor net charge current:

$$I_\uparrow + I_\downarrow = 0,$$
$$I_\uparrow - I_\downarrow = 0,$$

i.e.,

$$I_\uparrow = 0,\ I_\downarrow = 0.$$

Therefore, the definition of charge Seebeck coefficient should be[41]

$$S_c = -\left.\frac{\Delta V}{\Delta T}\right|_{I=0,I_s=0}$$

In other words, for systems with spin accumulation, the two spin channels are independent and the charge accumulation is the sum of individual accumulations. In this situation, the other thermal-spin quantities can be deduced straightforwardly. The electric conductance G_σ, the Seebeck coefficient of spin-σ S_σ, and the electronic contribution to the thermal conductance $k_{e,\sigma}$ are expressed by the transmission coefficient $\mathcal{T}_\sigma(\varepsilon)$ ($\hbar$ restored explicitly):

$$G_\sigma = \frac{e^2}{h}\int d\varepsilon\,(-f'_\varepsilon)|_{\mu,T}\mathcal{T}_\sigma(\varepsilon) = e^2 L_{0\sigma}, \tag{21}$$

$$S_\sigma = -\frac{1}{eT}\frac{\int d\varepsilon(\varepsilon-\mu)(-f'_\varepsilon)|_{\mu,T}\mathcal{T}_\sigma(\varepsilon)}{\int d\varepsilon(-f'_\varepsilon)|_{\mu,T}\mathcal{T}_\sigma(\varepsilon)} = -\frac{1}{eT}\frac{L_{1\sigma}}{L_{0\sigma}}, \tag{22}$$

$$k_{e,\sigma} = \frac{1}{T}\left(L_{2\sigma} - \frac{L_{1\sigma}^2}{L_{0\sigma}}\right), \tag{23}$$

where

$$L_{n\sigma} \equiv \frac{1}{h}\int d\varepsilon\,(\varepsilon-\mu)^n(-f'_\varepsilon)|_{\mu,T}\mathcal{T}_\sigma(\varepsilon),$$

and the referential electrochemical potential μ and temperature T are set as

$$\mu = \frac{1}{4}(\mu_{L\uparrow} + \mu_{L\downarrow} + \mu_{R\uparrow} + \mu_{R\downarrow}),\ T = \frac{1}{2}(T_L + T_R).$$

Using these quantities, the charge and spin thermoelectric coefficients are obtained from the following expressions,[26,42]

$$S_\mathrm{s} = S_\uparrow - S_\downarrow, \qquad G_\mathrm{s} = G_\uparrow - G_\downarrow, \tag{24}$$

$$S_\mathrm{c} = (S_\uparrow + S_\downarrow)/2,\ G_\mathrm{c} = G_\uparrow + G_\downarrow, \tag{25}$$

$$Z_\mathrm{s}T = |G_\mathrm{s}|\,S_\mathrm{s}^2 T/k_e, \tag{26}$$

$$Z_\mathrm{c}T = G_\mathrm{c}S_\mathrm{c}^2 T/k_e, \qquad k_e = k_{e\uparrow} + k_{e\downarrow}\ . \tag{27}$$

Note that there is an extra factor of 1/2 in Ref. 26 in the definition of spin-dependent Seebeck coefficient S_s,[43] resulting from a different definition of "spin voltage", μ_s. Here, we adopt the natural definition: $\mu_s = \mu_\uparrow - \mu_\downarrow$, which is generally accepted and widely used in the literature.[4,17,41,42,44]

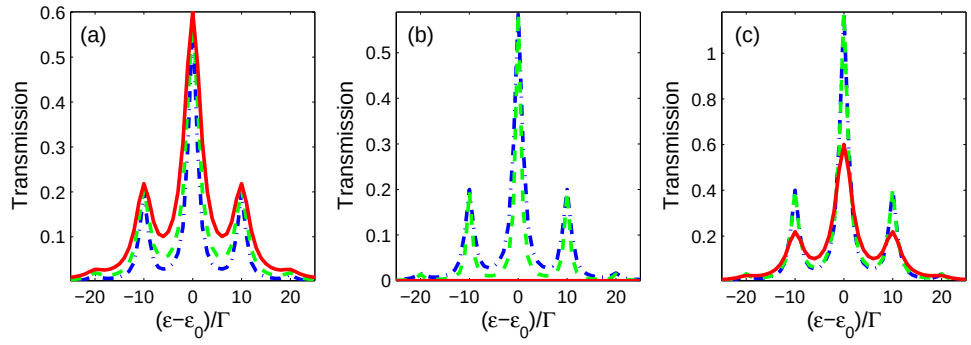

FIG. 3. (color online) Transmission coefficients of (a) spin-up, (b) spin-down electrons, and (c) both kinds of electrons of the single-level FM/QD/FM spin-valve in parallel configuration with different polarizations in leads, $p = 0$ (blue dash dotted line), 0.4 (green dashed line), 1 (red solid line). The AC bias is applied with $\hbar\omega = e\Delta = 10\,\Gamma$.

b. Without spin accumulation. If there is no spin accumulation in the FM leads due to spin relaxation, no spin voltage will be generated and the Seebeck coefficient is determined by the condition that the total charge current equals to zero, i.e., balanced by the external voltage bias and temperature bias:

$$S = -\left.\frac{\Delta V}{\Delta T}\right|_{I=0}.$$

In this case, the total transmission coefficient should be employed to calculate the corresponding thermoelectric quantities. And we have

$$G = \frac{e^2}{\hbar}\int \frac{d\varepsilon}{2\pi}\,(-f'_\varepsilon)\,|_{\mu,T}\mathcal{T}(\varepsilon) = e^2 L_0, \tag{28}$$

$$S = -\frac{1}{eT}\frac{\int d\varepsilon\,(\varepsilon-\mu)\,(-f'_\varepsilon)\,|_{\mu,T}\mathcal{T}(\varepsilon)}{\int d\varepsilon\,(-f'_\varepsilon)\,|_{\mu,T}\mathcal{T}(\varepsilon)} = -\frac{1}{eT}\frac{L_1}{L_0}, \tag{29}$$

$$k_e = \frac{1}{T}\left(L_2 - \frac{L_1^2}{L_0}\right), \tag{30}$$

where

$$\mathcal{T}(\varepsilon) = \sum_\sigma \mathcal{T}_\sigma(\varepsilon),$$

$$L_n \equiv \frac{1}{h}\int d\varepsilon\,(\varepsilon-\mu)^n\,(-f'_\varepsilon)\,|_{\mu,T}\mathcal{T}(\varepsilon).$$

Especially for spin degenerate cases, we can use the transmission coefficient of a single spin channel, $\mathcal{T}_\sigma(\varepsilon)$, and include the spin degeneracy by adding a factor 2 into the expressions of L_n.

For our problem of non-collinear spin-valves driven in AC fields, the above derived formulae appear rather similar to those of collinear magnetic structure in AC or non-collinear in DC. The differences lie in the content of the physical quantities such as transmission coefficients and linewidth functions. In this work we shall ignore the lattice thermal conductance since it is essentially a constant for small AC fields and for any noncollinearity θ of the magnetic tunnel junction. This approximation does not change the quantitative behaviors of the thermoelectric properties to be discussed below. Without the lattice contribution to thermal conductance, the absolute value of ZT doesn't correspond to those obtained in experiments. Therefore, we shall focus on the trends of ZT, i.e., how the qualitative trends are altered by the AC fields and under noncollinear magnetic structures.

III. NUMERICAL RESULTS AND DISCUSSION

Having derived the general expressions of thermoelectric properties for noncollinear magnetic tunnel junctions driven by an external AC bias, in the rest of the paper we investigate a specific FM/QD/FM system where the QD has a single spin-degenerate

level. For this model, all quantities associated with the QD become 2×2 matrices, and the trace in the effective transmission Eq. (18) needs only to go over spin degrees of freedom.

For clarity, we suppose that the two FM leads are made of the same material, having the same spin polarization such that the components of bandwidth functions in Eq. (11) are given by $\Gamma_{\alpha,\sigma} = \Gamma(1 + \sigma p)$. In the following, thermal-spin effects are presented and discussed first, followed by results of normal thermoelectric properties, among which dependencies on spin polarization, noncollinear angle, and AC frequency will be focused.

A. Transmission coefficients

While the behaviors of transmission coefficients of QD in many different situations have been well documented in the literature, for completeness and for later discussions (e.g., thermoelectric properties), we shall briefly discuss them in this subsection using Γ as the energy unit. We begin by considering the parallel ($\theta = 0$) configuration and non-polarized ($p = 0$) situation under the AC fields. For this case both spin channels have the same transport features and the total transmission coefficient is plotted in Fig. 2 as a function of energy.

As shown in Fig. 2(a), the DC transmission (black line, overlapping with the other lines) is in the expected Lorentzian line shape with a full width at half maximum equaling to Γ. The maximum of the total transmission is 2 and it occurs at $\varepsilon = \varepsilon_0$, due to the resonant tunneling through the two degenerate QD states. When a harmonic AC source with small amplitude $e\Delta/\hbar\omega = 0.1$ is applied, changes caused by the AC field immerse in the DC spectrum and are too small to decern. When $e\Delta/\hbar\omega = 1$, the photon-assisted features are more clearly seen, as illustrated in Fig. 2(b). First, there are side peaks located at

$$\varepsilon - \varepsilon_0 = k\hbar\omega, k = 0, 1, 2, \cdots . \tag{31}$$

These peaks are due to the well known k-photon-assisted tunneling[34,45] and each term in the summation of Eq. (18) can be viewed as the contribution from the k-photon process. As shown in the figure, transmission coefficient is symmetric about $|\varepsilon_0 - \mu| = 0$ (chemical potential μ is set to zero throughout). From the photon point of view, the left side of transmission coefficient is associated with first absorption and then emission of photons, while the right side, first emission and then absorption. Second, the major peak at $\varepsilon - \varepsilon_0 = 0$ is suppressed, and the peak heights of resonant tunneling become lower for larger k. The suppression is due to the prefactor $J_k^2(e\Delta/\hbar\omega)$ in each term of the summation in Eq. (18), and that $J_k^2(e\Delta/\hbar\omega)$ monotonically decreases with k when $e\Delta/\hbar\omega = 1$. In fact, for the parallel magnetic configuration, the DC transmission is determined by the density of states $\rho_\sigma(\varepsilon)$ of the QD as[39,46]

$$\mathcal{T}_\sigma(\varepsilon) = 2\pi \frac{\Gamma_{L\sigma}\Gamma_{R\sigma}}{\Gamma_{L\sigma} + \Gamma_{R\sigma}} \rho_\sigma(\varepsilon), \tag{32}$$

from which one finds that the total area under the transmission curve is a constant that only depends on the linewidth parameters,

$$\int \mathcal{T}_\sigma(\varepsilon) d\varepsilon = 2\pi\Gamma_{L\sigma}\Gamma_{R\sigma} / (\Gamma_{L\sigma} + \Gamma_{R\sigma}). \tag{33}$$

When the AC bias is applied, the transmission is a weighted sum with weighting factors $J_k^2(e\Delta/\hbar\omega)$. Since the total weight equals to one,[47]

$$\sum\nolimits_k J_k^2(\alpha) = 1, \tag{34}$$

the total area under the transmission coefficient for the AC case is the same as that for the DC case. In other words, the transmission probability is redistributed over the whole spectrum. This well explains why the main peak is suppressed under AC. In fact, in Appendix D we prove that the area is not influenced by the AC bias (within WBL approximation) even for noncollinear magnetic tunnel junctions. A main effect of an AC bias is therefore to redistribute the transmission spectrum for both collinear and noncollinear magnetic structures. Increasing the amplitude parameter of the AC bias further, e.g., to $e\Delta/\hbar\omega = 10$, heights of the photon-assisted side peaks may overshoot the main peak, and particular side peaks may disappear as well due to the oscillation of the function $J_k^2(\alpha)$ with k, as shown in Fig. 2(c).

The spin polarization p of the FM/QD/FM spin-valve also has significant impact on the transmission spectrum. As plotted in Fig. 3, transmission coefficients of the two spin channels are equal when $p = 0$, but become quite different as p is increased. Fig. 3(a) shows that transmission of the majority spin decreases with increasing p; Fig. 3(b) shows that the opposite is true for the minority spin. This behavior can be understood as follows. When $p = 0$ (normal metal), there is no difference in transmission between the two spin channels hence $\mathcal{T}_\uparrow(\varepsilon) = \mathcal{T}_\downarrow(\varepsilon)$. For $p = 1$ (half metal), only the majority spin can tunnel through the QD

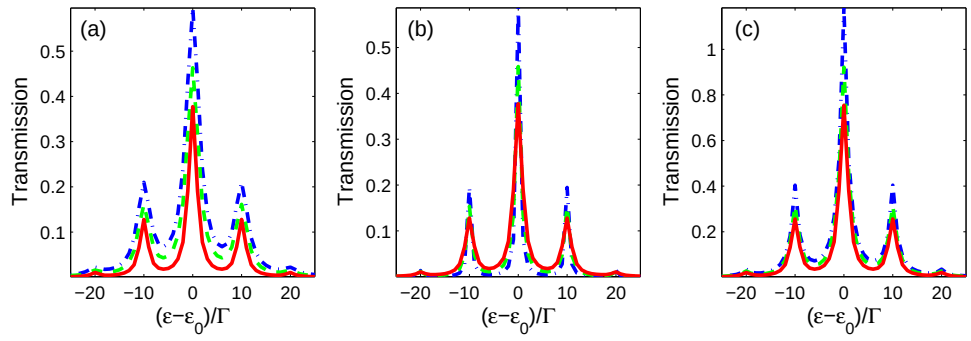

FIG. 4. (color online) Transmission coefficients of (a) spin-up, (b) spin-down electrons, and (c) both kinds of electrons of the FM/QD/FM device with different angles of the magnetic moments of the leads, $\theta = 0$ (blue dash dotted), 0.5π (green dashed), π (red solid), under AC bias with $\hbar\omega = e\Delta = 10\,\Gamma$, and $p = 0.6$.

region, so $\mathcal{T}_\uparrow(\varepsilon) = 1$ and $\mathcal{T}_\downarrow(\varepsilon) = 0$. These limits determine the general trends of transmission coefficients when polarization in leads increases from zero to one. By contrast, total transmission has smoother variation as p increases, resembling $\mathcal{T}_\uparrow$ as shown in Fig. 3(c). Importantly, Fig. 3 shows that decreasing p can make the transmission peaks (in the total transmission) much sharper thus enhancing the derivatives of the transmission function so as to change the Seebeck coefficients. In addition, increasing (decreasing) p makes the transmission peaks of minority-spin (majority-spin) channel sharper. We conclude that FM/QD/FM spin-valves made of different FM materials should have rather different Seebeck coefficients due to different polarizations.

Now let's look at the impact of the alignment of the leads' magnetic moments. In Fig. 4, the transmission function is plotted as a function of energy at different noncollinearity angles θ. Quite different from changing the polarization, varying the spin-valve rotation angle gives rise to remarkable variation of resonant peak heights. As θ increases from 0 to π, transmission of spin-up electrons is suppressed and transmission of the spin-down electrons is enhanced. Such a spin-valve behavior is well known from the Julliere model.[48] As θ increases, the energy derivative of $\mathcal{T}_\uparrow$ gradually increases, that of $\mathcal{T}_\downarrow$ decreases; and the total transmission has faster variation with ε as θ increases. These variations finally result in different dependencies for spin-valve systems with or without spin accumulation as we shall see below. In next subsections, we shall mainly investigate which angle, polarization, and frequency are best for thermal-spin and normal thermoelectric properties.

B. Thermal-spin properties

It is interesting to investigate how noncollinear magnetic moments influence the Seebeck coefficients under the AC fields. Fig. 5 plots the Seebeck coefficients of spin-up ($S_\uparrow$) and spin-down ($S_\downarrow$) electrons, together with spin-dependent Seebeck (S_s) and charge (S_c) Seebeck coefficients. These quantities are calculated using the corresponding expressions in Section II B. All of them are 2π-periodic functions of θ, and are symmetric about $\theta = \pi$ because of the spatial symmetry of the spin-valve. As shown in Fig. 5, the Seebeck coefficient $S_\downarrow$ (blue dots) achieves its maximum at $\theta = 0$ (PC), and its minimum at $\theta = \pi$ (APC). Among the interval $[0, \pi]$, $S_\downarrow$ monotonically decreases with θ. In contrast, $S_\uparrow$ has the opposite trend. According to the Mott's relation discussed in the introduction, faster changes in transmission produce a higher Seebeck coefficient. Since resonant transmission of minority spin at PC is unity regardless of polarization as long as $p \neq 1$,[49] and is generally lowest at other energy points at PC, $[\mathcal{T}_\downarrow(\varepsilon)]'_\varepsilon$ is biggest at PC, also shown in Fig. 4. That is why $S_\downarrow$ has the maximum value at $\theta = 0$ and $S_\uparrow$ has the opposite behavior.

As an average of $S_\uparrow$ and $S_\downarrow$, the charge Seebeck coefficient S_c has a weaker dependence on θ. Interestingly and rather unexpectedly, the maximum of S_c appears at $\theta = 0$, which means PC is actually better for obtaining a larger charge Seebeck coefficient. The spin-dependent Seebeck coefficient S_s also has the maximum value (largest negative value) at PC and decreases with increasing angle until $\theta = \pi$, where $S_s = 0$. The zero value of S_s is because that $\mathcal{T}_\uparrow(\varepsilon) = \mathcal{T}_\downarrow(\varepsilon)$ for our symmetric spin-valve when $\theta = \pi$, and then S_s vanishes by Eq. (24). We also observe that S_c and S_s are of the the same order and of opposite signs, which implies that they are mainly determined by $S_\downarrow$.

What alignment of the magnetic moments of the spin-valve is better for enhancing the Seebeck coefficients? As shown in Fig. 6, for the case of at $\varepsilon_0 = -10\ \mu$eV, both charge and spin-dependent Seebeck coefficients achieve their maxima at parallel configuration, regardless of the polarization in the leads. It is also shown that Seebeck coefficients at $\theta = \pi$ are independent of polarization, a fact attributed to the spin-independent transmission at APC. In general, a higher polarization favors higher Seebeck coefficients for other noncollinear angles.

Next, we investigate the variation of off-resonance Seebeck coefficients and figures of merit on AC frequency. Here, off-

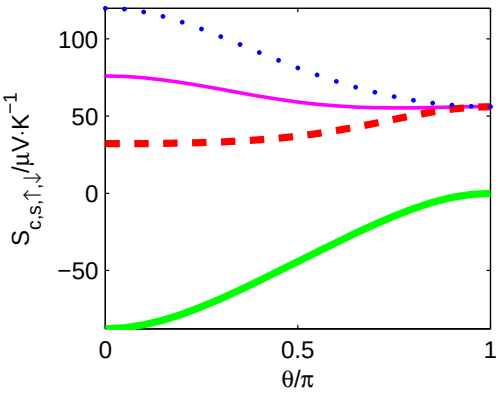

FIG. 5. (color online) Charge Seebeck (thin pink solid line), spin-dependent Seebeck (thick green solid line), spin-up Seebeck (red dashed line), and spin-down Seebeck (blue dotted line) coefficients as functions of θ. Other parameters are chosen to be $\Gamma = 10\ \mu$eV, $p = 0.6$, $\varepsilon_0 = -10\ \mu$eV, $T = 0.03$ K, $\omega = 25$ GHz, and $e\Delta/\hbar\omega = 1$.

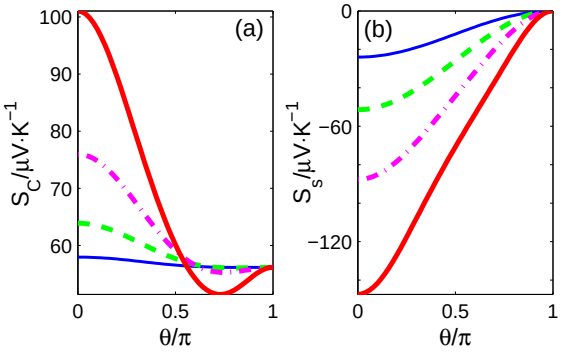

FIG. 6. (color online) (a) Charge Seebeck coefficient and (b) spin-dependent Seebeck coefficient as functions of θ at different polarizations of the leads, $p = 0.2$ (blue solid thin line), $p = 0.4$ (green dashed line), $p = 0.6$ (pink dash dotted line), and $p = 0.8$ (red solid thick line). The other parameters are set to be $\omega = 25$ GHz, $e\Delta/\hbar\omega = 1$, $\Gamma = 10\ \mu$eV, $\varepsilon_0 = -10\ \mu$eV, and $T = 0.03$ K.

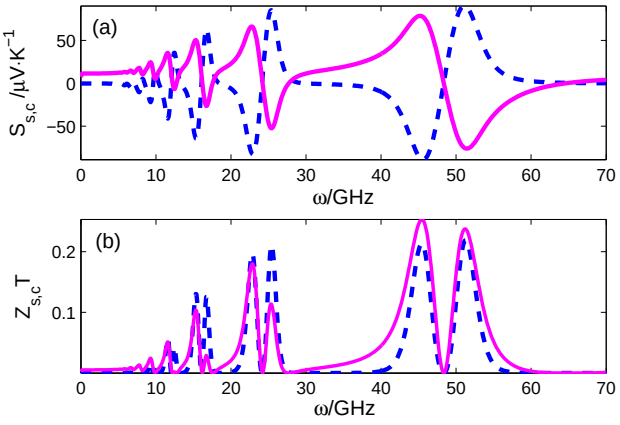

FIG. 7. (color online) Spin-dependent (blue dashed) and charge (pink solid) (a) Seebeck coefficients and (b) figures of merit as functions of the AC frequency ω. The QD level locates at $\varepsilon_0 = -200\ \mu$eV, and the AC bias is applied with $e\Delta/\hbar = 25$ GHz fixed, meaning constant power. Other parameters are chosen as $p = 0.6$, $\Gamma = 10\ \mu$eV, $\theta = 0$, and $T = 0.03$ K.

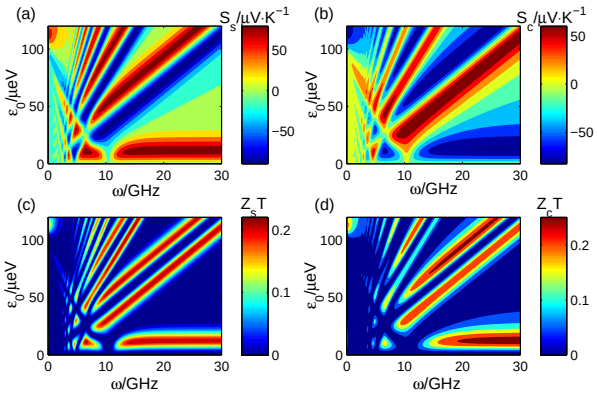

FIG. 8. (color online) Contour plots of (a) spin-dependent Seebeck coefficient, (b) charge Seebeck coefficient, (c) spin figure of merit, and (d) charge figure of merit, as functions of level position ε_0 and AC frequency ω. The amplitude of AC bias Δ is fixed at $e\Delta/\hbar = 25$ GHz. Other parameters are chosen to be $\Gamma = 10$ μeV, $p = 0.6, \theta = 0, T = 0.03$ K.

resonance means electron energy $\varepsilon \neq \varepsilon_0$ where ε_0 is the energy level of the QD. It is found that there is photon-induced magnetoresistance oscillation in tunneling systems as shown in Ref. 50. What about thermoelectric properties? Should them monotonically change with the applied frequency or have similar oscillation? In Fig. 7, we plot $S_{c,s}$ and $Z_{c,s}T$ as functions of ω. The spin-dependent Seebeck coefficient S_s is nearly independent of ω for small ω. When ω increases to moderate values, S_s starts to vary around its DC value and the variation becomes greater when ω increases further. At around $\omega \sim |\varepsilon_0 - \mu|$ and larger, S_s reaches its largest peak and finally falls back to approach the DC value when ω further increases. Interestingly, the charge Seebeck coefficient S_c has essentially the same oscillatory behavior, but its peaks and valleys occur out-of-phase with those in S_s. This variation of S_s and S_c versus ω is in fact consistent with the variation of the transmission coefficient $\mathcal{T}(\varepsilon)$. When $\hbar\omega \sim |\varepsilon_0 - \mu|$, single-photon-assisted tunneling enhances $\mathcal{T}(\varepsilon)$, showing an 1-photon-assisted side peak around the chemical potential μ, leading to significant values of Seebeck coefficients. Especially for $\hbar\omega = (1-\delta)(\mu - \varepsilon_0)$, $\delta \ll 1$, μ locates at the right-hand side of the first side peak, leading to a positive value of S, while for $\hbar\omega = (1+\delta)(\mu - \varepsilon_0)$, $\delta \ll 1$, the left-hand side, leading to negative S. Importantly, Seebeck coefficients vanish at the middle of a symmetric transmission spectrum due to electron-hole symmetry, so it is nearly zero at the middle of a transmission peak provided that thermal smearing is less than the peak width. Therefore, a side peak will introduce an oscillation in S as a function of AC frequency. In fact, the k-photon-assisted will have major contributions to $\mathcal{T}(\varepsilon)$ or current when $k\hbar\omega = |\varepsilon_0 - \mu|$, or $\omega = (1/\hbar)|\varepsilon_0 - \mu|/k$. There are dense photon-assisted tunneling peaks when ω is very small. Side peaks in $\mathcal{T}(\varepsilon)$ generally have lower peak heights and overlap with each other, resulting in tiny changes of S. This is the reason why $S_{c,s}$ are rather flat when ω is small. When $\hbar\omega > |\varepsilon_0 - \mu|$, which means the energy of a single photon is larger than the difference between the QD level position and the chemical potential, there is hardly any photon-assisted tunneling; And as a consequence, oscillation of S disappears.

There are also oscillations in Z_cT and Z_sT as shown in Fig. 7(b). The zeros of $Z_{c/s}T$ is the same as those in $S_{c/s}$, originating from the relations shown in Eqs. (26) and (27). An oscillation in $S_{c/s}$ generally corresponds to two peaks of $Z_{c/s}T$ because $Z_{c/s}T \propto S^2_{c/s}$. It is also shown that a larger $S_{c/s}$ is better for a larger ZT. From Fig. 7(b), it is clear that the single-photon-assisted tunneling is of most significance for $Z_{c/s}T$.

The behaviors of Seebeck coefficients and figures of merit versus the QD energy level position (ε_0) and AC frequency (ω) are summarized in the contour plot of Fig. 8. When ε_0 is close to the chemical potential, applying an AC bias lowers the major peak in the transmission spectrum, yielding a suppression of Seebeck coefficient. As shown in Fig. 8(a), there are pairs of peaks and valleys around each line of $\varepsilon_0 = k\hbar\omega$. The region where $\omega < 6$ GHz is rather flat as we have addressed before. S_c in Fig. 8(b) has smoother variation than S_s. What's more, the opposite signs and trends of S_c and S_s can be seen clearly from the two panels (peaks and valleys of S_c and S_s are out of phase). Note that S_c and S_s are of the same order. Spin and charge figures of merit are plotted in Fig. 8(c) and (d). Compared to the Seebeck coefficients, the photon-assisted resonance features are more clearly standing-out. For the region $\omega < 2.5$ GHz ≈ 10 μeV$= \Gamma$ and $\varepsilon_0 < \Gamma$, both Z_sT and Z_cT are almost zero because the changes caused by the AC field immerse in the original main resonance peak.

It is intriguing and important to point out that the photon-assisted $Z_{c,s}T$ peaks - i.e., those due to photon side peaks in the transmission coefficients, have the same order of values as those due to the main resonance peak of $\mathcal{T}(\varepsilon)$, as shown in Figs. 8(c) and (d). Although the photon-assisted peaks in $\mathcal{T}(\varepsilon)$ are much lower than the main resonance peak in $\mathcal{T}(\varepsilon)$ as depicted in Figs. 3 and 4, transmission peak heights have little influence on the maximum of $Z_{c,s}T$. Combining with the Mott's relation, we can conclude that a general scaling on the transmission has almost no effect on $S_{c,s}$ and on $Z_{c,s}T$ when κ_e dominates the thermal conductance.

Finally, we have also investigated other non-collinearity angles. For APC, S_s is always zero while S_c oscillates with the

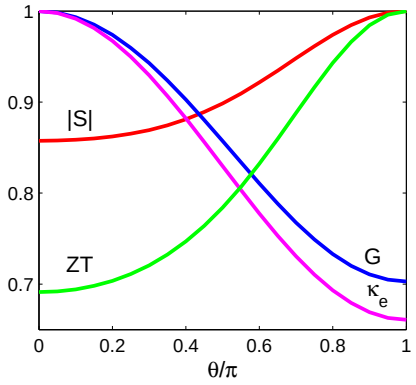

FIG. 9. (color online) Normalized thermoelectric quantities $|S|$ (red line), G (blue line), κ_e (magenta line), and ZT (green line) as functions of θ. The normalizing factors are $S_m = 58.6\,\mu$V/K, $G_m = 0.172\times(2e^2/h)$,$\kappa_{e,m} = 4.97\times10^{-6}$ nW/K, and $ZT_m = 0.146$. Here, the QD level position is supposed to be $\varepsilon_0 = -115\,\mu$eV. The other parameters are $\Gamma = 10\,\mu$eV, $T = 0.03$ K, $\omega = 25$ GHz, $e\Delta/\hbar\omega = 1$, and $p = 0.6$.

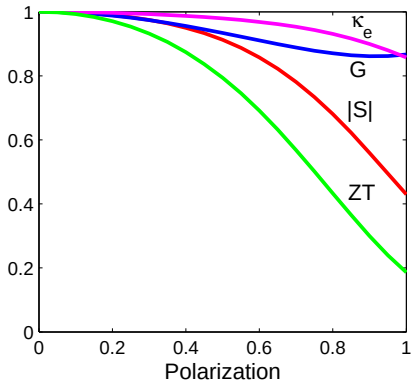

FIG. 10. (color online) Normalized thermoelectric quantities $|S|$ (red line), G (blue line), κ_e (magenta line), and ZT (green line) as functions of leads' polarization. The normalizing factors are $S_m = 58.6\,\mu$V/K, $G_m = 0.189\times(2e^2/h)$,$\kappa_{e,m} = 5.13\times10^{-6}$ nW/K, and $ZT_m = 0.146$. The other parameters are $\Gamma = 10\,\mu$eV, $T = 0.03$ K, $\omega = 25$ GHz, $e\Delta/\hbar\omega = 1$, $\theta = 0$, and $\varepsilon_0 = -115\,\mu$eV.

AC frequency, similar to what is reported above. In general, oscillations of $S_{c,s}$ and $Z_{c,s}T$ on ω are commonly found in other non-collinear angles.

C. Thermoelectric Properties

In this subsection we investigate the normal thermoelectric effects where there is no spin accumulation in the FM leads. In this situation, the total transmission due to both spin channels is employed to calculate the thermoelectric quantities. As addressed before, the angular and polarization dependencies are quite different between the total transmission and the individual spin channels.

As shown in Fig. 9, we fix the QD level position at $\varepsilon_0 = -115\,\mu$eV, which is in the vicinity of the first photon-assisted peak of Seebeck coefficient under an 25 GHz AC bias (25 GHz $\approx 103\,\mu$eV). Two major features can be seen from this figure. First, all quantities monotonically vary with θ. $|S|$ and ZT have their maximum values at APC and the minima at PC, which are totally different from the spin-dependent case discussed in the last subsection. On the other hand, the electrical conductance G and electronic thermal conductance κ_e have similar variations, and both have the maximum values at PC. When the temperature is low enough, κ_e has essentially the same behavior as G, which is consistent with known literature.[51] Second, the calculated magneto-thermopower, defined as MTP$\equiv (S_{AP} - S_P)/S_P$, is about 16% which is qualitatively consistent with experiments.[3,5] We may therefore conclude that the APC is best for enhancing the normal thermoelectric properties.

As for the variation of polarization, we plot the normalized thermoelectric properties in Fig. 10 at PC. The changes in G and κ_e due to polarization p are small because the summation over the two spin channels largely averages out the effect of p. On the other hand, $|S|$ and ZT decrease fast as polarization p increases, hence non-polarized leads are better for higher ZT values.

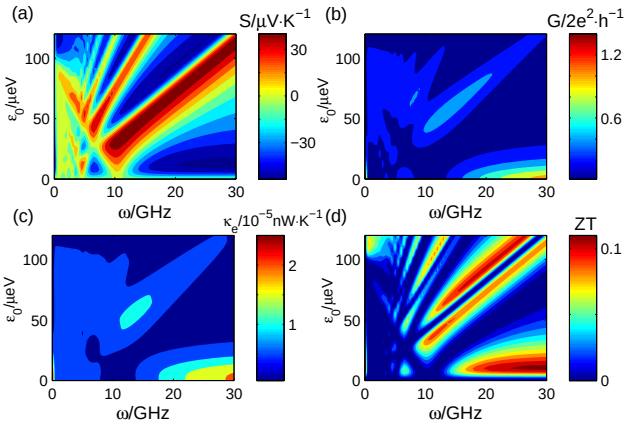

FIG. 11. (color online) Thermoelectric properties in spin-valve where no spin accumulates in the leads. Contour plots of (a) Seebeck coefficient, (b) electric conductance, (c) thermal conductance, and (d) figure of merit ZT, as functions of AC frequency ω, and the quantum dot level position, ε_0. Other parameters are chosen as $\theta = 0$, $\Gamma = 10\ \mu$eV, $p = 0.6$, $e\Delta/\hbar = 25$ GHz.

TABLE I. The calculated DC values of parallel and antiparallel Seebeck coefficients (with no spin-accumulation) for a QD spin-valve having a spin-degenerated energy level. The experimental values are quoted from Ref. 22. The parameters are chosen to be $\Gamma = 10\ \mu$eV, $T = 0.03$ K, and $p = 0.6$.

	TMR	$S_P(\mu$V/K)	$S_{AP}(\mu$V/K)
This work	76%	44.4	54.5
Ref. 22	76%	22	53

Finally, the frequency dependence of the physical quantities G, κ_e, S, and ZT are plotted in Fig. 11, for parallel spin-valve ($\theta = 0$) with $p = 0.6$. The impressive radial pattern is also observed resembling those of the spin-dependent case (see Fig. 8). However, the AC-induced variations in G and κ_e are much weaker here than the spin case, which also results in the similarity of S and ZT.

So far we have focused on varying model parameters to establish a general physical picture for the transport properties of the FM/QD/FM spin-valve under external AC fields. To make better comparison with experiments, we choose linewidth parameter $\Gamma = 10\ \mu$eV, which is a typical experimental value for QD devices,[30,39] $p = 0.6$, which is the polarization for FM alloy CoFeB,[52] ω about tens of GHz - the range of frequency in and beyond microwaves, and $T = 0.03$ K (or $k_BT \approx 4.3\ \mu$eV). Although a lower temperature usually means a lower ZT, here we are interested in the low temperature fine structures of quantum origin such as photon-assisted resonant tunneling in the temperature scale of $k_BT \ll \Gamma, \omega$. Using these realistic parameter values in Eq. (25), the calculated normal Seebeck coefficients are found to be quite close to those measured in experiments,[22] as shown in Table III C. Given the substantial differences in device structures and materials, the quantitative consistency is quite reasonable.

IV. SUMMARY

In summary, we have carried out a theoretical analysis of thermal-spin and thermoelectric properties of non-collinear spin-valves driven by a high frequency AC voltage bias. A general and exact formulation for the time-averaged physical properties of the spin-valve model is derived by the nonequilibrium Green's function theory in the linear response regime under the wide-band limit, and the analytic formulation provides a starting point for further numerical calculations of these properties. We find that non-collinear FM/QD/FM spin-valves under harmonic AC bias have very interesting thermal-spin and thermoelectric properties which can be tuned by several control parameters. It is shown that photon-assisted tunneling processes manifest clearly in the transmission spectra, and strongly depend on the magnetic polarization and magnetic configuration.

For thermal-spin effects, both spin-dependent and charge Seebeck coefficients S_s and S_c generally achieve their maximum absolute values at parallel magnetic configuration, and the domination of minority-spin Seebeck coefficient leads to opposite signs and opposite variations of S_s and S_c. On the other hand, for normal thermoelectric effects, S and ZT achieve the maxima at anti-parallel configuration of the spin-valve. For both thermal-spin and normal thermoelectric effects, when an AC bias with a moderate frequency is applied, S and ZT oscillate around their DC value as the AC frequency is increased due to photon-assisted tunneling. At higher frequency, these quantities go back to their DC values. The microscopic details behind these behaviors are discussed based on the transmission coefficients. It is found that the area under the transmission spectrum is a

constant even under the AC bias, which provides a constraint on the variation of the thermoelectric properties. Finally, we note that the oscillation behavior of the thermoelectric properties of the spin-valve driven by an AC bias offers a "knob" to tune the thermoelectric behaviors of magnetic tunneling junction.

Finally, we note that the electron-electron and electron-phonon interactions are not considered in our device model. The former gives rise to interesting phenomena of the Coulomb blockade and Kondo resonance in QD systems while the latter is needed for exactly determining the lattice thermal conductivity at high temperature. Adding these terms to the device Hamiltonian will make the analysis significantly more complicated but these effects clearly warrant further investigations. Since our numerical results of the device model showed very reasonable consistency with the experimental results, the general formalism of Sec. II may be extended further to better explore the AC thermoelectric properties in magnetic tunneling junctions.

ACKNOWLEDGEMENT

We thank Prof. C.-M. Hu for many useful discussions concerning their experimental data reported in Ref. 22 as well as on general issues of thermal-spin effects in magnetic tunnel junctions, and also thank Qing Shi, Jingzhe Chen, Yibin Hu for helpful discussions. We gratefully acknowledge financial support of NSERC of Canada (H.G.). X.B.C. acknowledges a visiting scholarship of Tsinghua University. W.H.D. is supported by NSF-China (grant No. 11074139), and by MST-China (grant No. 2011CB921901 and 2011CB606405).

Appendix A: spin-polarized current

Some of the derivation details of Section II are organized in several appendices below. We first derive expressions for the spin-polarized current. As defined in Eq. (1), the Hamiltonian is

$$H = H_L + H_C + H_R + H_T.$$

To calculate the electric current, we consider the change of the number of electrons $N_{L/R}$ in the leads as

$$\hat{N}_{L/R} = \sum_{ks,\alpha\in L/R} C^\dagger_{k\alpha s} C_{k\alpha s}, \tag{A1}$$

$$\begin{aligned} J_L &= -e\left\langle \frac{d\hat{N}_L}{dt}\right\rangle = ie\left\langle \left[\hat{N}_L, H\right]\right\rangle = ie\left\langle \left[\hat{N}_L, H_T\right]\right\rangle \\ &= ie\sum_{ksn\sigma,\alpha\in L}\left[t_{k\alpha s,n\sigma}\left\langle C^\dagger_{k\alpha s} d_{n\sigma}\right\rangle - t^*_{k\alpha s,n\sigma}\left\langle d^\dagger_{n\sigma} C_{k\alpha s}\right\rangle\right] \\ &= e\sum_{ksn\sigma,\alpha\in L}\left[t_{k\alpha s,n\sigma} G^<_{n\sigma,k\alpha s}(t,t) - t^*_{k\alpha s,n\sigma} G^<_{k\alpha s,n\sigma}(t,t)\right] \\ &= 2e\,\mathrm{Re}\sum_{ksn\sigma,\alpha\in L} t_{k\alpha s,n\sigma} G^<_{n\sigma,k\alpha s}(t,t), \end{aligned} \tag{A2}$$

where the lesser Green's functions are defined as

$$G^<_{n\sigma,k\alpha s}(t,t') = \frac{1}{i}\left\langle T_t\left(d_{n\sigma}(t)\, C^\dagger_{k\alpha s}(t')\right)\right\rangle = i\left\langle C^\dagger_{k\alpha s}(t')\, d_{n\sigma}(t)\right\rangle \tag{A3}$$

$$G^<_{k\alpha s,n\sigma}(t,t') = \frac{1}{i}\left\langle T_t\left(C_{k\alpha s}(t)\, d^\dagger_{n\sigma}(t')\right)\right\rangle = i\left\langle d^\dagger_{n\sigma}(t')\, C_{k\alpha s}(t)\right\rangle, \tag{A4}$$

and have the relation $\left[G^<_{n\sigma,k\alpha s}(t,t)\right]^\dagger = -G^<_{k\alpha s,n\sigma}(t,t)$.

Regarding the expression of total current in Eq. (A2), it is natural to introduce a spin-resolved current as

$$J_{L,s\sigma} \equiv 2e\,\mathrm{Re}\sum_{n,k,\alpha\in L} t_{k\alpha s,n\sigma} G^<_{n\sigma,k\alpha s}(t,t), \tag{A5}$$

which accounts for the contribution from the spin-s electrons in lead L tunneling to the QD as spin-σ. Then the spin-s current and the total current are $J_{L,s} = \sum_\sigma J_{L,s\sigma}$ and $J_L = \sum_{s,\sigma} J_{L,s\sigma}$, respectively.

Using Eq. (A5) , we shall express the current in terms of bandwidth functions in the following. First, from the Dyson equation, we have

$$\begin{aligned} G_{n\sigma,k\alpha s}(t,t') &= \sum_{n',\sigma'} \int d\tau_1 G_{n\sigma,n'\sigma'}(t,\tau_1)\, t_{n'\sigma',k\alpha s} g_{k\alpha s}(\tau_1,t') \\ &= \sum_{n',\sigma'} \int d\tau_1 G_{n\sigma,n'\sigma'}(t,\tau_1)\, t^*_{k\alpha s,n'\sigma'} g_{k\alpha s}(\tau_1,t'). \end{aligned}$$

Applying the Lengreth theorem, we obtain

$$\begin{aligned} G^<_{n\sigma,k\alpha s}(t,t) = &\sum_{n',\sigma'} \int d\tau_1 G^r_{n\sigma,n'\sigma'}(t,\tau_1)\, t^*_{k\alpha s,n'\sigma'} g^<_{k\alpha s}(\tau_1,t) \\ &+ \sum_{n',\sigma'} \int d\tau_1 G^<_{n\sigma,n'\sigma'}(t,\tau_1)\, t^*_{k\alpha s,n'\sigma'} g^a_{k\alpha s}(\tau_1,t). \end{aligned} \tag{A6}$$

For noninteracting and isolated leads, the Green's functions are[34]

$$\begin{aligned} g^<_{k\alpha s}(\tau_1,t) &= if\left(\varepsilon^0_{k\alpha s}\right) e^{-i\varepsilon^0_{k\alpha s}(\tau_1-t)} e^{-i\int_t^{\tau_1}\Delta_\alpha(\tau)d\tau}, \\ g^a_{k\alpha s}(\tau_1,t) &= i\theta(t-\tau_1)\, e^{-i\varepsilon^0_{k\alpha s}(\tau_1-t)} e^{-i\int_t^{\tau_1}\Delta_\alpha(\tau)d\tau}. \end{aligned} \tag{A7}$$

Substitute Eq. (A7) into Eq. (A6) and replace the summation over k, $\sum_k$, by integration over energy, $\int d\varepsilon \rho(\varepsilon)$, we have

$$\begin{aligned} &\sum_{k,\alpha\in L} t_{k\alpha s,n\sigma} G^<_{n\sigma,k\alpha s}(t,t) \\ =&i\sum_{\alpha\in L}\int d\varepsilon \rho_{\alpha s}(\varepsilon) t_{\alpha s,n\sigma}(\varepsilon) \sum_{n'\sigma'}\int_{-\infty}^{t} d\tau_1 G^r_{n\sigma,n'\sigma'}(t,\tau_1) \\ &\cdot t^*_{\alpha s,n'\sigma'}(\varepsilon)\cdot f_\alpha(\varepsilon) e^{-i\varepsilon(\tau_1-t)} e^{-i\int_t^{\tau_1}\Delta_\alpha(\tau)d\tau} \\ &+ i\sum_{\alpha\in L}\int d\varepsilon \rho_{\alpha s}(\varepsilon) t_{\alpha s,n\sigma}(\varepsilon) \sum_{n'\sigma'}\int_{-\infty}^{t} d\tau_1 G^<_{n\sigma,n'\sigma'}(t,\tau_1) \\ &\cdot t^*_{\alpha s,n'\sigma'}(\varepsilon)\cdot e^{-i\varepsilon(\tau_1-t)} e^{-i\int_t^{\tau_1}\Delta_\alpha(\tau)d\tau} \\ =&i\int \frac{d\varepsilon}{2\pi}\sum_{n'\sigma'} \mathbf{\Gamma}_{Ls;n'\sigma',n\sigma}(\varepsilon)\int_{-\infty}^{t} d\tau_1 e^{-i\varepsilon(\tau_1-t)} e^{-i\int_t^{\tau_1}\Delta_\alpha(\tau)d\tau} \\ &\cdot\left[G^r_{n\sigma,n'\sigma'}(t,\tau_1)\cdot f_\alpha(\varepsilon) + G^<_{n\sigma,n'\sigma'}(t,\tau_1)\right], \end{aligned}$$

where the spin-s bandwidth function $\mathbf{\Gamma}_{Ls}$ is defined as

$$\mathbf{\Gamma}_{Ls;n'\sigma',n\sigma}(\varepsilon) \equiv 2\pi\sum_{\alpha\in L}\rho_{\alpha s}(\varepsilon)\, t_{\alpha s,n\sigma}(\varepsilon)\, t^*_{\alpha s,n'\sigma'}(\varepsilon). \tag{A8}$$

Under WBL, which neglects the energy dependence of bandwidth functions, the integration involving $G^<$ can be carried out:

$$\begin{aligned} J_{L,s\sigma} = &-2e\,\mathrm{Im}\,\mathrm{Tr}\left\{\int\frac{d\varepsilon}{2\pi}\sum_{\sigma'}\mathbf{\Gamma}_{Ls;\sigma'\sigma}\right. \\ &\left.\cdot\int_{-\infty}^{t} d\tau_1 G^r_{\sigma,\sigma'}(t,\tau_1)\cdot f_L(\varepsilon) e^{-i\varepsilon(\tau_1-t)} e^{-i\int_t^{\tau_1}\Delta_L(\tau)d\tau}\right\} \\ &- e\,\mathrm{Im}\,\mathrm{Tr}\sum_{\sigma'}\mathbf{\Gamma}_{Ls;\sigma'\sigma} G^<_{\sigma,\sigma'}(t,t), \end{aligned} \tag{A9}$$

where the trace goes over orbital degrees of freedom, and

$$\begin{aligned} J_{L,s} = &-\frac{2e}{\hbar}\int_{-\infty}^{t} d\tau_1\int\frac{d\varepsilon}{2\pi} f_L(\varepsilon)\,\mathrm{Im}\,\mathrm{Tr}\{ \\ &e^{-i\varepsilon(\tau_1-t)} e^{-i\int_t^{\tau_1}\Delta_L(\tau)d\tau}\mathbf{\Gamma}_{L,s} G^r(t,\tau_1)\Big\} - \frac{e}{\hbar}\,\mathrm{Im}\,\mathrm{Tr}\,\mathbf{\Gamma}_{L,s} G^<(t,t), \end{aligned} \tag{A10}$$

tracing over both spin and orbital degrees of freedom.

Appendix B: Retarded Green's function of the QD

For further calculation, we need to calculate the retarded Green's function of the central region. By Dyson equation, we have

$$G^r(t,t') = G_0^r(t,t') + \iint G_0^r(t,t_1)\,\Sigma^r(t_1,t_2)\,G^r(t_2,t')\,dt_1dt_2, \tag{B1}$$

where G_0^r is the retarded Green's function of the isolated QD (i.e. no electrodes), and the retarded self-energy under WBL can be written as[34]

$$\Sigma^r(t_1,t_2) = -\frac{i}{2}\mathbf{\Gamma}\delta(t_1-t_2). \tag{B2}$$

The time-dependent retarded Green's function of the isolated QD can be obtained by

$$G_0^r(t,t') = G_0^r(t-t') = \int \frac{dE}{2\pi} G_0^r(E)\,e^{-iE(t-t')}, \tag{B3}$$

$$G_0^r(E) = [E + i\eta - H_0]^{-1}, \tag{B4}$$

where H_0 is the Hamiltonian of the isolated QD.

In virtue of Eqs. (B2) and (B3), Eq. (B1) can be rewritten as

$$G^r(t,t') = G_0^r(t-t') + \int G_0^r(t-t_1)(-\frac{i}{2}\mathbf{\Gamma})G^r(t_1,t')\,dt_1.$$

To get an analytic form, we carry out the double-Fourier transform:

$$\begin{aligned}
&G^r(E,E') = \iint G^r(t,t')\,e^{iEt}e^{-iE't'}\,dtdt' \\
&= 2\pi G_0^r(E)\,\delta(E-E') - \\
&\frac{i}{2}\iiint G_0^r(t-t_1)\,e^{iE(t-t_1)}e^{-iE't'}e^{iEt_1}\mathbf{\Gamma}G^r(t_1,t')\,dt_1dtdt' \\
&= 2\pi G_0^r(E)\,\delta(E-E') - \frac{i}{2}G_0^r(E)\,\mathbf{\Gamma}G^r(E,E') \\
&= 2\pi\delta(E-E')\sum_{n=0}^{+\infty}\left(-\frac{i}{2}G_0^r(E)\,\mathbf{\Gamma}\right)^n G_0^r(E) \\
&\equiv 2\pi\delta(E-E')\,G^r(E),
\end{aligned}$$

where we have defined $G^r(E)$ as

$$\begin{aligned}
G^r(E) &\equiv \sum_{n=0}^{+\infty}\left(-\frac{i}{2}G_0^r(E)\,\mathbf{\Gamma}\right)^n G_0^r(E) = \sum_{n=0}^{+\infty} G_0^r(E)\left(-\frac{i}{2}\mathbf{\Gamma}G_0^r(E)\right)^n \\
&= G_0^r(E) + G_0^r(E)\left(-\frac{i}{2}\mathbf{\Gamma}\right)G^r(E).
\end{aligned}$$

It shows that $G^r(E)$ and $G_0^r(E)$ have a Dyson-equation-type connection.

Since $G_0^r(E)$ can be obtained by Eq. (B4), $G^r(E)$ defined above can be obtained similarly by

$$G^r(E) = [E + i\eta - H_0 - \Sigma^r]^{-1} = \left[E + i\eta - H_0 + \frac{i}{2}\mathbf{\Gamma}\right]^{-1}. \tag{B5}$$

There are two auxiliaries that we shall use afterwards.

(1) $G^r(t,t')$ is now expressed in terms of $G^r(E)$ as

$$\begin{aligned}
G^r(t,t') &= \int\frac{dE}{2\pi}\int\frac{dE'}{2\pi}G^r(E,E')\,e^{-iEt}e^{iE't'} \\
&= \int\frac{dE}{2\pi}\int\frac{dE'}{2\pi}2\pi\delta(E-E')\,G^r(E)\,e^{-iEt}e^{iE't'} \\
&= \int\frac{dE}{2\pi}G^r(E)\,e^{-iE(t-t')}.
\end{aligned} \tag{B6}$$

(2)

$$G^r(E) - G^a(E) = -iG^r(E)\mathbf{\Gamma}G^a(E). \tag{B7}$$

Using Eq. (B5), we have

$$[G^r(E)]^{-1} - [G^a(E)]^{-1} = i\mathbf{\Gamma}.$$

Multiplying the above equation on both sides by $G^r(E)$ from the left and $G^a(E)$ from the right, we obtain Eq. (B7), which is actually an identity relation without assuming the WBL.

Appendix C: $\langle J \rangle$

To facilitate the calculation of time averaged current, we shall deduce an explicit expression for currents in a multi-level QD under harmonic modulation. First, the Keldysh equation gives

$$G^<(t,t) = \iint G^r(t,t_1)\Sigma^<(t_1,t_2)G^a(t_2,t)\,dt_2dt_1,$$

where the lesser self-energy from definition is

$$\Sigma^<(t_1,t_2) = V^\dagger(t_1)g^<(t_1,t_2)V(t_2).$$

Substitute Eq. (A7) to the above equation, we obtain the lesser self-energy as

$$\begin{aligned}&\Sigma^<_{m\sigma,n\sigma'}(t_1,t_2)\\ &= \sum_{\alpha=L,R}\int\frac{d\varepsilon}{2\pi}if_\alpha(\varepsilon)e^{-i\varepsilon(t_1-t_2)}e^{-i\int_{t_2}^{t_1}\Delta_\alpha(\tau)d\tau}\mathbf{\Gamma}_{\alpha;m\sigma,n\sigma'}\end{aligned} \tag{C1}$$

with $\mathbf{\Gamma}_{\alpha;m\sigma,n\sigma'} = \sum_s \mathbf{\Gamma}_{\alpha s;m\sigma,n\sigma'}$, where $\mathbf{\Gamma}_{\alpha s}$ is defined in Eq. (A8).

Accordingly, the lesser Green's function can be simplified as

$$\begin{aligned}G^<(t,t) &= \iint G^r(t,t_1)\sum_{\alpha=L,R}\int\frac{d\varepsilon}{2\pi}if_\alpha(\varepsilon)e^{-i\varepsilon(t_1-t_2)}e^{-i\int_{t_2}^{t_1}\Delta_\alpha(\tau)d\tau}\\ &\quad\cdot\mathbf{\Gamma}_\alpha G^a(t_2,t)\,dt_2dt_1\\ &= \sum_{\alpha=L,R} i\int\frac{d\varepsilon}{2\pi}f_\alpha(\varepsilon)A_\alpha(\varepsilon,t)\mathbf{\Gamma}_\alpha A^\dagger_\alpha(\varepsilon,t),\end{aligned} \tag{C2}$$

where the spectral function $A_\alpha(\varepsilon,t)$ is defined as[34]

$$A_\alpha(\varepsilon,t) \equiv \int_{-\infty}^{+\infty} dt_1 G^r(t,t_1)e^{-i\varepsilon(t_1-t)}e^{-i\int_t^{t_1}\Delta_\alpha(\tau)d\tau}, \tag{C3}$$

and

$$\begin{aligned}A_\alpha(\varepsilon,t)\mathbf{\Gamma}_\alpha A^\dagger_\alpha(\varepsilon,t) &= \int_{-\infty}^{+\infty} dt_1 G^r(t,t_1)e^{-i\varepsilon(t_1-t)}e^{-i\int_t^{t_1}\Delta_\alpha(\tau)d\tau}\\ &\quad\cdot\mathbf{\Gamma}_\alpha\int_{-\infty}^{+\infty} dt_2 G^a(t_2,t)e^{i\varepsilon(t_2-t)}e^{i\int_t^{t_2}\Delta_\alpha(\tau)d\tau}\\ &= \int_{-\infty}^{+\infty} dt_2\int_{-\infty}^{+\infty} dt_1 G^r(t,t_1)\mathbf{\Gamma}_\alpha\\ &\quad\cdot G^a(t_2,t)e^{-i\varepsilon(t_1-t_2)}e^{-i\int_{t_2}^{t_1}\Delta_\alpha(\tau)d\tau}.\end{aligned} \tag{C4}$$

With Eqs. (C2) and (C3), the time dependent spin-polarized current can be written in terms of $A_\alpha(\varepsilon,t)$:

$$\begin{aligned}J_{L,\sigma}(t) = &-e\sum_{\alpha=L,R}\int\frac{d\varepsilon}{2\pi}f_\alpha(\varepsilon)\mathrm{Tr}[\mathbf{\Gamma}_{L,\sigma}A_\alpha(\varepsilon,t)\mathbf{\Gamma}_\alpha A^\dagger_\alpha(\varepsilon,t)]\\ &-2e\int\frac{d\varepsilon}{2\pi}f_L(\varepsilon)\,\mathrm{Im}\,\mathrm{Tr}\left[\mathbf{\Gamma}_{L,\sigma}A_L(\varepsilon,t)\right].\end{aligned} \tag{C5}$$

Noting that Γ_α is a real and symmetric matrix, the quantity $\mathrm{Tr}(A_\alpha \mathbf{\Gamma}_\alpha A_\alpha^\dagger)$ is real.

Using the expression for G^r in Eq. (B6), the spectral function is actually

$$\begin{aligned}
A_\alpha(\varepsilon,t) &\equiv \int_{-\infty}^{+\infty} dt_1 G^r(t,t_1)\, e^{-i\varepsilon(t_1-t)} e^{ie\Delta_\alpha \int_t^{t_1}\cos\omega\tau d\tau} \\
&= \int_{-\infty}^{+\infty} dt_1 \int \frac{dE}{2\pi} G^r(E)\, e^{-iE(t-t_1)} e^{-i\varepsilon(t_1-t)} e^{i\frac{e\Delta_\alpha}{\omega}(\sin\omega t_1 - \sin\omega t)} \\
&= e^{-i\frac{e\Delta_\alpha}{\omega}\sin\omega t} \int \frac{dE}{2\pi} e^{it(\varepsilon-E)} G^r(E) \\
&\quad \cdot \int_{-\infty}^{+\infty} dt_1 e^{it_1(E-\varepsilon)} \sum_{k=-\infty}^{+\infty} J_k\left(\frac{e\Delta_\alpha}{\omega}\right) e^{ik\omega t_1} \\
&= \sum_{k=-\infty}^{+\infty} J_k\left(\frac{e\Delta_\alpha}{\omega}\right) e^{it(\varepsilon-E)} e^{-i\frac{e\Delta_\alpha}{\omega}\sin\omega t} \\
&\quad \cdot \int \frac{dE}{2\pi} G^r(E)\, 2\pi\delta(E-\varepsilon+k\omega) \\
&= \sum_{k=-\infty}^{+\infty} J_k\left(\frac{e\Delta_\alpha}{\omega}\right) e^{ik\omega t} e^{-i\frac{e\Delta_\alpha}{\omega}\sin\omega t} G^r(\varepsilon-k\omega),
\end{aligned}$$

where we have adopted an identity expansion relation for the first kind Bessel function that $\exp(iz\sin\omega t) = \sum_k J_k(z)\exp(ik\omega t)$. Performing time-averaging, we have

$$\begin{aligned}
\langle A_\alpha(\varepsilon,t)\rangle &= \sum_k J_k^2\left(\frac{e\Delta_\alpha}{\omega}\right) G^r(\varepsilon-k\omega), \\
\mathrm{Im}\,\langle A_\alpha(\varepsilon,t)\rangle &= \sum_k J_k^2\left(\frac{e\Delta_\alpha}{\omega}\right) \mathrm{Im}\, G^r(\varepsilon-k\omega) \\
&= -\frac{1}{2}\sum_k J_k^2\left(\frac{e\Delta_\alpha}{\omega}\right) G^r(\varepsilon-k\omega)\mathbf{\Gamma} G^a(\varepsilon-k\omega).
\end{aligned} \tag{C6}$$

Note that in the last equation, Eq. (B7) has been utilized.

Similarly,

$$\begin{aligned}
&A_\alpha(\varepsilon,t)\mathbf{\Gamma}_\alpha A_\alpha^\dagger(\varepsilon,t) \\
&= \sum_k J_k\left(\frac{e\Delta_\alpha}{\omega}\right) e^{ik\omega t} e^{-i\frac{e\Delta_\alpha}{\omega}\sin\omega t} G^r(\varepsilon-k\omega) \\
&\quad \cdot \mathbf{\Gamma}_\alpha \sum_{k'} J_{k'}\left(\frac{e\Delta_\alpha}{\omega}\right) e^{-ik'\omega t} e^{i\frac{e\Delta_\alpha}{\omega}\sin\omega t} G^a(\varepsilon-k\omega) \\
&= \sum_{k,k'} J_k\left(\frac{e\Delta_\alpha}{\omega}\right) J_{k'}\left(\frac{e\Delta_\alpha}{\omega}\right) e^{i(k-k')\omega t} G^r(\varepsilon-k\omega)\cdot\mathbf{\Gamma}_\alpha G^a(\varepsilon-k\omega) \\
&\left\langle A_\alpha(\varepsilon,t)\mathbf{\Gamma}_\alpha A_\alpha^\dagger(\varepsilon,t)\right\rangle \\
&= \sum_k J_k^2\left(\frac{e\Delta_\alpha}{\omega}\right) G^r(\varepsilon-k\omega)\cdot\mathbf{\Gamma}_\alpha G^a(\varepsilon-k\omega).
\end{aligned} \tag{C7}$$

Then the time-averaged current is found to be

$$\begin{aligned}
J_{L,\sigma} &\equiv \langle J_{L,\sigma}(t)\rangle \\
&= -e\sum_{\alpha=L,R}\int\frac{d\varepsilon}{2\pi}f_\alpha(\varepsilon)\sum_k J_k^2\left(\frac{e\Delta_\alpha}{\omega}\right) \\
&\quad\cdot \mathrm{Tr}[\mathbf{\Gamma}_{L,\sigma}G^r(\varepsilon-k\omega)\cdot\mathbf{\Gamma}_\alpha G^a(\varepsilon-k\omega)] \\
&\quad + e\int\frac{d\varepsilon}{2\pi}f_L(\varepsilon)\sum_k J_k^2\left(\frac{e\Delta_L}{\omega}\right) \\
&\quad\cdot \mathrm{Tr}\left[\mathbf{\Gamma}_{L,\sigma}G^r(\varepsilon-k\omega)\mathbf{\Gamma}G^a(\varepsilon-k\omega)\right] \\
&= e\int\frac{d\varepsilon}{2\pi}\sum_k\left[f_L(\varepsilon)J_k^2\left(\frac{e\Delta_L}{\omega}\right)-f_R(\varepsilon)J_k^2\left(\frac{e\Delta_R}{\omega}\right)\right] \\
&\quad\cdot \mathrm{Tr}\left[\mathbf{\Gamma}_{L,\sigma}G^r(\varepsilon-k\omega)\mathbf{\Gamma}_R G^a(\varepsilon-k\omega)\right].
\end{aligned} \tag{C8}$$

In particular, when $\Delta_L = \Delta_R \equiv \Delta$, we obtain

$$\begin{aligned}
J_{L,\sigma} = e\int\frac{d\varepsilon}{2\pi}\left[f_L(\varepsilon)-f_R(\varepsilon)\right]\sum_k J_k^2\left(\frac{e\Delta}{\omega}\right) \\
\cdot \mathrm{Tr}\left[\mathbf{\Gamma}_{L,\sigma}G^r(\varepsilon-k\omega)\mathbf{\Gamma}_R G^a(\varepsilon-k\omega)\right].
\end{aligned} \tag{C9}$$

Appendix D: Area Under the Transmission Curve

As shown in Eq. (18) above, the transmission spectrum for general cases is

$$\mathcal{T}_\sigma(\varepsilon) = \sum_k J_k^2\left(\frac{e\Delta}{\omega}\right)\mathrm{Tr}\left[\mathbf{\Gamma}_{L,\sigma}G^r(\varepsilon-k\omega)\mathbf{\Gamma}_R G^a(\varepsilon-k\omega)\right].$$

The pre-factor J_k is independent of energy, so the integration over energy of $\mathcal{T}_\sigma(\varepsilon)$ becomes

$$\begin{aligned}
A_{AC} &= \int\mathcal{T}_\sigma(\varepsilon)\,d\varepsilon \\
&= \sum_k J_k^2\left(\frac{e\Delta}{\omega}\right)\int d\varepsilon\,\mathrm{Tr}\left[\mathbf{\Gamma}_{L,\sigma}G^r(\varepsilon-k\omega)\mathbf{\Gamma}_R G^a(\varepsilon-k\omega)\right] \\
&= \sum_k\left[J_k^2\left(\frac{e\Delta}{\omega}\right)\right]\int d\varepsilon\,\mathrm{Tr}\left[\mathbf{\Gamma}_{L,\sigma}G^r(\varepsilon)\mathbf{\Gamma}_R G^a(\varepsilon)\right] \\
&= \int d\varepsilon\,\mathrm{Tr}\left[\mathbf{\Gamma}_{L,\sigma}G^r(\varepsilon)\mathbf{\Gamma}_R G^a(\varepsilon)\right] \\
&= A_{DC},
\end{aligned}$$

where $\sum_k J_k^2(z) \equiv 1$.[47] Therefore, the total area under the transmission spectrum is independent of the AC frequency and equal to that of the DC case under WBL.

* xbchen@physics.mcgill.ca

[1] G. J. Snyder and E. S. Toberer, Nat. Mater. **7**, 105 (2008).
[2] Y. Dubi and M. Di Ventra, Rev. Mod. Phys. **83**, 131 (2011).
[3] M. Walter, J. Walowski, V. Zbarsky, M. Münzenberg, M. Schäfers, D. Ebke, G. Reiss, A. Thomas, P. Peretzki, M. Seibt, J. S. Moodera, M. Czerner, M. Bachmann, and C. Heiliger, Nat. Mater. **10**, 742 (2011).
[4] G. E. W. Bauer, E. Saitoh, and B. J. van Wees, Nat. Mater. **11**, 391 (2012).
[5] W. Lin, M. Hehn, L. Chaput, B. Negulescu, S. Andrieu, F. Montaigne, and S. Mangin, Nat. Commun. **3**, 744 (2012).
[6] F. J. DiSalvo, Science **285**, 703 (1999).
[7] R. Mahajan, C. Chia-pin, and G. Chrysler, Proc. IEEE **94**, 1476 (2006).
[8] C. B. Vining, Nat. Mater. **8**, 83 (2009).
[9] P. Murphy, S. Mukerjee, and J. Moore, Phys. Rev. B **78**, 161406 (2008).
[10] M. S. Dresselhaus, G. Chen, M. Y. Tang, R. G. Yang, H. Lee, D. Z. Wang, Z. F. Ren, J. P. Fleurial, and P. Gogna, Adv. Mater. **19**, 1043 (2007).
[11] M. Cutler and N. F. Mott, Phys. Rev. **181**, 1336 (1969).
[12] M. Paulsson and S. Datta, Phys. Rev. B **67**, 241403 (2003).
[13] P. Reddy, S.-Y. Jang, R. A. Segalman, and A. Majumdar, Science **315**, 1568 (2007).
[14] F. Mazzamuto, V. Hung Nguyen, Y. Apertet, C. Caër, C. Chassat, J. Saint-Martin, and P. Dollfus, Phys. Rev. B **83**, 235426 (2011).
[15] K. K. Saha, T. Markussen, K. S. Thygesen, and B. K. Nikolić, Phys. Rev. B **84**, 041412 (2011).
[16] G. D. Mahan and J. O. Sofo, Proc. Natl. Acad. Sci. U.S.A. **93**, 7436 (1996).
[17] K. Uchida, S. Takahashi, K. Harii, J. Ieda, W. Koshibae, K. Ando, S. Maekawa, and E. Saitoh, Nature **455**, 778 (2008).
[18] M. Meschke, W. Guichard, and J. Pekola, Nature **444**, 187 (2006).
[19] T. Ojanen and A.-P. Jauho, Phys. Rev. Lett. **100**, 155902 (2008).
[20] L. M. A. Pascal, H. Courtois, and F. W. J. Hekking, Phys. Rev. B **83**, 125113 (2011).
[21] C. Feng and D. B. Yonatan, J. Phys.: Condens. Matter **24** (2012).
[22] Z. H. Zhang, Y. S. Gui, L. Fu, X. L. Fan, J. W. Cao, D. S. Xue, P. P. Freitas, D. Houssameddine, S. Hemour, K. Wu, and C.-M. Hu, Phys. Rev. Lett. **109**, 037206 (2012).
[23] M. N. Baibich, J. M. Broto, A. Fert, F. N. Van Dau, F. Petroff, P. Etienne, G. Creuzet, A. Friederich, and J. Chazelas, Phys. Rev. Lett. **61**, 2472 (1988).
[24] J. C. Slonczewski, Phys. Rev. B **39**, 6995 (1989).
[25] H. Mehrez, J. Taylor, H. Guo, J. Wang, and C. Roland, Phys. Rev. Lett. **84**, 2682 (2000).
[26] R. Swirkowicz, M. Wierzbicki, and J. Barnas, Phys. Rev. B **80**, 195409 (2009).
[27] J. Zheng, F. Chi, and Y. Guo, J. Phys.: Condens. Matter **24**, 265301 (2012).
[28] L. P. Kouwenhoven, S. Jauhar, J. Orenstein, P. L. McEuen, Y. Nagamune, J. Motohisa, and H. Sakaki, Phys. Rev. Lett. **73**, 3443 (1994).
[29] T. H. Oosterkamp, L. P. Kouwenhoven, A. E. A. Koolen, N. C. van der Vaart, and C. J. P. M. Harmans, Phys. Rev. Lett. **78**, 1536 (1997).
[30] T. H. Oosterkamp, T. Fujisawa, W. G. van der Wiel, K. Ishibashi, R. V. Hijman, S. Tarucha, and L. P. Kouwenhoven, Nature **395**, 873 (1998).
[31] K. Shibata, A. Umeno, K. M. Cha, and K. Hirakawa, Phys. Rev. Lett. **109**, 077401 (2012).
[32] N. Liebing, S. Serrano-Guisan, K. Rott, G. Reiss, J. Langer, B. Ocker, and H. W. Schumacher, Phys. Rev. Lett. **107**, 177201 (2011).
[33] B. Wang, J. Wang, and H. Guo, J. Phys. Soc. Jpn. **70**, 2645 (2001).
[34] A.-P. Jauho, N. S. Wingreen, and Y. Meir, Phys. Rev. B **50**, 5528 (1994).
[35] Q.-F. Sun and T.-H. Lin, Phys. Rev. B **56**, 3591 (1997).
[36] J. Martinek, Y. Utsumi, H. Imamura, J. Barnaś, S. Maekawa, J. König, and G. Schön, Phys. Rev. Lett. **91**, 127203 (2003).
[37] N. Sergueev, Q.-F. Sun, H. Guo, B. Wang, and J. Wang, Phys. Rev. B **65**, 165303 (2002).
[38] P. Zhang, Q.-K. Xue, Y. Wang, and X. C. Xie, Phys. Rev. Lett. **89**, 286803 (2002).
[39] Y. Meir, N. S. Wingreen, and P. A. Lee, Phys. Rev. Lett. **70**, 2601 (1993).
[40] H. Lu, R. Lu, and B.-F. Zhu, J. Phys.: Condens. Matter **18**, 8961 (2006).
[41] T. Rejec, R. Žitko, J. Mravlje, and A. Ramšak, Phys. Rev. B **85**, 085117 (2012).
[42] Y. Dubi and M. Di Ventra, Phys. Rev. B **79**, 081302 (2009).
[43] S_s was also called spin Seebeck coefficient in the literature.
[44] A. Slachter, F. Bakker, J. Adam, and B. Van Wees, Nat. Phys. **6**, 879 (2010).
[45] P. K. Tien and J. P. Gordon, Phys. Rev. **129**, 647 (1963).
[46] Γ_α^{-1} can be viewed as the finite lifetime of an electron staying in the QD before transmitting into lead α or vice versa. Therefore, the time for an electron to transmit from lead L to lead R is about $\tilde{\Gamma}^{-1} = \Gamma_L^{-1} + \Gamma_R^{-1}$, which leads to $\tilde{\Gamma} = \Gamma_L\Gamma_R/(\Gamma_L + \Gamma_R)$. And further, the escaping rate $\tilde{\Gamma}/\hbar$ timing the effective density of states $(-1/\pi)\mathrm{Im}G^r$ gives us roughly the transmission.
[47] Using the identity $e^{i\alpha\sin\omega t} = \sum_{k=-\infty}^{+\infty} J_k(\alpha)\, e^{ik\omega t}$, we have $1 = |e^{i\alpha\sin\omega t}|^2 = \sum_k J_k^2(\alpha) + \sum_{k\neq k'} J_k(\alpha)\, J_{k'}(\alpha)\, e^{i(k-k')\omega t}$. In light of the abitrary value of t, it can be seen that $\sum_{k\neq k'} J_k(\alpha)\, J_{k'}(\alpha)\, e^{i(k-k')\omega t} = 0$ and $\sum_k J_k^2(\alpha) = 1$.
[48] M. Julliere, Phys. Lett. A **54**, 225 (1975).
[49] Since there is no minority-spin electrons in the leads when $p = 1$, $\mathcal{T}(\varepsilon) \equiv 0$. Actually in this case, $S_\downarrow$ and S_s are not well-defined by Eqs. (22) and (24).
[50] R. Mani, A. Ramanayaka, and W. Wegscheider, Phys. Rev. B **84**, 085308 (2011).
[51] Z.-C. Wang, G. Su, and S. Gao, Phys. Rev. B **63**, 224419 (2001).

[52] D. D. Djayaprawira, K. Tsunekawa, M. Nagai, H. Maehara, S. Yamagata, N. Watanabe, S. Yuasa, Y. Suzuki, and K. Ando, Appl. Phys. Lett. **86**, 092502 (2005).